Stem Cell Reports
Report
ISSCR
OPEN ACCESS

s-SHIP Promoter Expression Identifies Mouse Mammary Cancer Stem Cells

Lu Tian,[1] Marie-José Truong,[1] Chann Lagadec,[2] Eric Adriaenssens,[2] Emmanuel Bouchaert,[3] Hélène Bauderlique-Le Roy,[4] Martin Figeac,[5] Xuefen Le Bourhis,[2] and Roland P. Bourette[1,*]

[1]Université de Lille, CNRS, Institut Pasteur de Lille, UMR 8161 - M3T - Mechanisms of Tumorigenesis and Targeted Therapies, Institut de Biologie de Lille, 1 rue du Professeur Calmette, CS 54447, Lille Cedex 59000/59021, France
[2]Université de Lille, INSERM U908 - CPAC - Cell Plasticity and Cancer, Lille 59000, France
[3]Oncovet Clinical Research, SIRIC ONCOLille, Loos 59120, France
[4]BICeL Platform, Institut Pasteur de Lille, Lille 59000, France
[5]Functional Genomics Platform, Université de Lille, Lille 59000, France
*Correspondence: roland.bourette@ibl.cnrs.fr
https://doi.org/10.1016/j.stemcr.2019.05.013

SUMMARY

During normal mammary gland development, s-SHIP promoter expression marks a distinct type of mammary stem cells, at two different stages, puberty and early mid-pregnancy. To determine whether s-SHIP is a marker of mammary cancer stem cells (CSCs), we generated bitransgenic mice by crossing the C3(1)-SV40 T-antigen transgenic mouse model of breast cancer, and a transgenic mouse (11.5kb-GFP) expressing green fluorescent protein from the s-SHIP promoter. Here we show that in mammary tumors originating in these bitransgenic mice, s-SHIP promoter expression enriches a rare cell population with CSC activity as demonstrated by sphere-forming assays *in vitro* and limiting dilution transplantation *in vivo*. These s-SHIP-positive CSCs are characterized by lower expression of Delta-like non-canonical Notch ligand 1 (DLK1), a negative regulator of the Notch pathway. Inactivation of *Dlk1* in s-SHIP-negative tumor cells increases their tumorigenic potential, suggesting a role for DLK1 in mammary cancer stemness.

INTRODUCTION

Breast cancer is the leading cause of cancer-related death among females across the world. It is a highly complex disease marked by genetic and clinical heterogeneity (Torre et al., 2015). Intertumoral heterogeneity of breast cancers led to a classification into several subsets with varied patient outcomes and implications for treatment. This heterogeneity is associated with an epithelial hierarchy in tumors resembling that observed in normal mammary gland. On top of this hierarchy that forms the tumor bulk is a cell subpopulation described as cancer stem cells (CSCs) or tumor-initiating cells (TICs) (Al-Hajj et al., 2003; Ginestier et al., 2007). CSCs are defined as cells that retain extensive self-renewal potential through a series of generations and have the ability to recreate the heterogeneity of the original tumor through asymmetric division (Nassar and Blanpain, 2016). The nature of breast CSCs is complex, with the demonstration of their heterogeneity both within and between breast tumors and the discovery of their plasticity (Sreekumar et al., 2015). Strong evidence has suggested that they are responsible for the recurrence, metastasis, and drug resistance of high-grade tumors (Peitzsch et al., 2017). A better understanding of breast CSCs might, therefore, provide prognostic information for relapse and metastasis and lead to the development of more efficient therapies.

Genetically engineered mouse models have been extremely important in helping to elucidate the mechanisms of pathogenesis of breast cancer (Menezes et al., 2014). Different CSC subpopulations have been identified in these transgenic mouse models of mammary carcinogenesis using combinations of cell-surface markers, such as $Lin^{-}CD29^{hi}CD24^{hi}$ (Zhang et al., 2008), $Thy1^{+}CD24^{+}$ (Cho et al., 2008), $CD29^{hi}CD24^{med}$ (Shafee et al., 2008), and CD61 (Vaillant et al., 2008). However, most of the sorting schemes require multiparameter fluorescence-activated cell sorting (FACS), yield sometimes rather heterogeneous cell populations, and are unclear in their biological meaning (Medema, 2013). Due to the general lack of unique cell-surface markers, the development of new markers to prospectively identify putative CSCs is of the utmost importance (Brooks et al., 2015).

Stem cell-specific expression of s-SHIP (stem-SH2-containing 5′-inositol phosphatase) was initially identified in embryonic and hematopoietic stem cells (Tu et al., 2001). A transgenic mouse (Tg 11.5kb-GFP or s-SHIP-GFP) was generated using the 11.5-kb s-SHIP promoter that specifically expresses enhanced green fluorescent protein (GFP) in several stem cell populations during embryonic development, including skin epidermis, hair follicles, mammary gland, and prostate (Rohrschneider et al., 2005). In the mammary gland, s-SHIP/GFP labels puberty cap cells and pregnancy basal alveolar bud cells, with a stem cell potential (Bai and Rohrschneider, 2010). Notably, s-SHIP expression in cap cells is associated with the expression of Par3-like polarity protein, which is essential for mammary stem cell maintenance (Huo and Macara, 2014).

The C3(1)/SV40 T-antigen transgenic mouse model (Tg C3(1)-Tag mice) develops mammary hyperplasia by 3 months of age with subsequent development of mammary adenocarcinoma by 5–6 months of age (Maroulakou et al., 1994). C3(1)-Tag mouse is a murine model of human

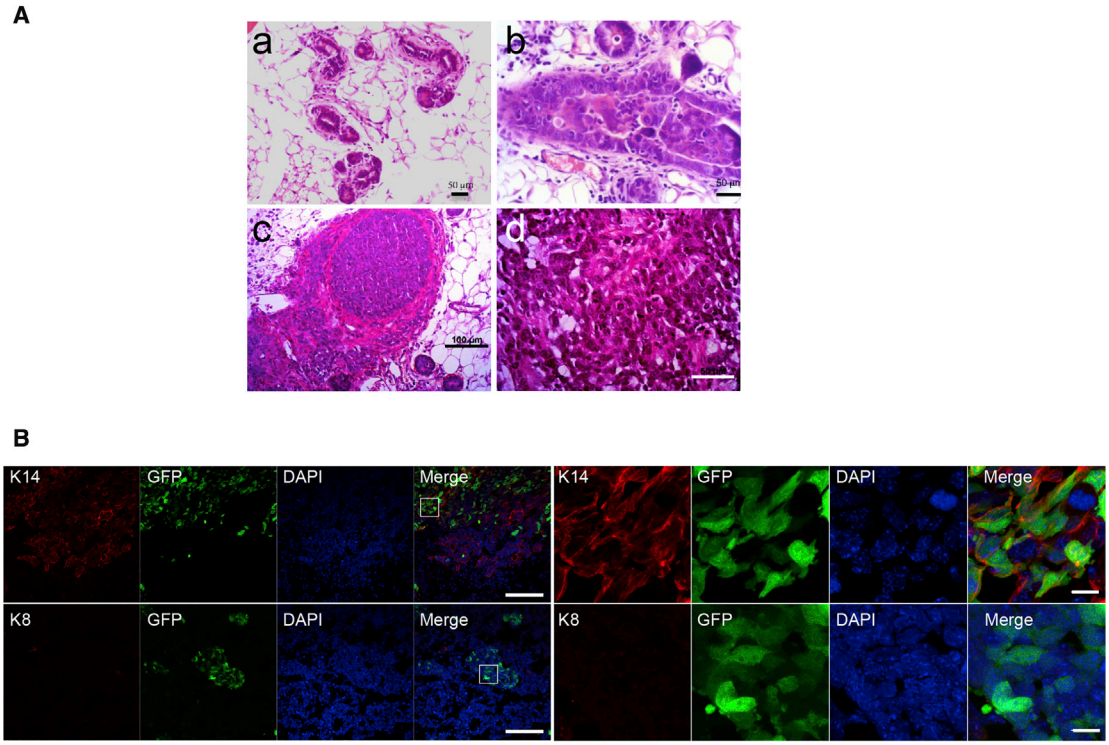

(legend on next page)

basal-like breast cancer, a complex group of breast cancers with both basal and luminal features (Dontu and Ince, 2015; Gusterson and Eaves, 2018). Using a cross-species genomics approach, murine expression profiles were compared with human breast cancers. The vast majority (≈90%) of the C3(1)-Tag mammary tumors displayed characteristics of human basal-like breast cancer, and 5%–10% showed the claudin-low subtype feature (Herschkowitz et al., 2007; Pfefferle et al., 2013; Usary et al., 2016), demonstrating the model's strong resemblance to human disease.

Here we aim to assess whether s-SHIP promoter expression could enable the isolation of a subpopulation of tumor cells with CSC characteristics, i.e., higher ability to self-renew and to form spheres *in vitro*, and higher ability to form secondary tumors phenotypically similar to the primary tumor, following their transplantation into immunodeficient mice. By crossing Tg 11.5kb-GFP mice with Tg C3(1)-Tag mice, we showed the presence of a subpopulation of GFP$^+$ cells in mammary tumors. These GFP$^+$ mammary cancer cells are CD24$^+$/CD49f$^+$/CD29$^+$, and enriched for sphere-forming activity *in vitro*. Importantly, they can regenerate heterogeneous tumors that display properties similar to the primary tumor upon subsequent transplantation. Transcriptomic analysis showed that these s-SHIP-positive CSCs were characterized by lower expression of Delta-like non-canonical Notch ligand 1 (DLK1), a negative regulator of the Notch pathway. Inactivation of *Dlk1* in s-SHIP-negative tumor cells increased their sphere-forming capacity and their tumorigenic potential, suggesting a role for DLK1 in mammary cancer cell stemness. Altogether, these results demonstrate that s-SHIP promoter expression offers a valuable marker for the isolation and characterization of mammary CSCs.

RESULTS

s-SHIP-GFP/C3(1)-Tag Bitransgenic Mice Develop Mammary Tumors Containing a Rare s-SHIP/GFP$^+$ Cell Subpopulation

We generated a bitransgenic mouse model by crossing homozygous Tg 11.5kb-GFP mice with hemizygous Tg C3(1)-Tag mice. Progressive mammary gland lesions were observed in female mice that carried the T Ag-containing transgene, from ductal hyperplasia to adenocarcinoma (Figures 1A and S1A). All female mice developed multiple mammary tumors by 4–5 months of age. GFP$^+$ cells were detected on frozen sections (Figure 1B) and by flow cytometry after enzymatic digestion of tumors (Figure 1C) (1.03% ± 0.64% of total cells, n = 10). The vast majority of GFP$^+$ cells were negative for lineage markers (Lin$^+$GFP$^+$ cells = 0.08% ± 0.08% of total cells, n = 5). These results indicated that s-SHIP promoter drives GFP expression specifically in a subpopulation of mammary tumor cells. Moreover, GFP expression correlated with the endogenous s-SHIP mRNA expression, since sorted tumor GFP$^+$ cells expressed higher levels of s-SHIP mRNA compared with sorted tumor GFP$^-$ cells (Figure S1C). Analysis of luminal (cytokeratin 8, K8) and basal/myoepithelial (cytokeratin 14, K14) markers showed that few tumors expressed K8 while all tumors displayed expression of K14 (Figure 1B). Importantly, GFP$^+$ tumor cells expressed K14 (Figure 1B). Similarly to s-SHIP/GFP expression at puberty during normal mammary gland development (Bai and Rohrschneider, 2010), some K14$^+$ mammary basal cells of 7-week-old bitransgenic mice also expressed GFP (Figure S1B). We next examined the expression of cell-surface markers historically associated with stem/progenitor cells in the mammary gland. Previous studies using flow cytometry to isolate mouse mammary stem cells have shown the majority of these cells to have a CD49f^{hi}CD29^{hi}CD24$^+$ EpCAM$^+$Sca-1^{neg} cell-surface marker phenotype (Shackleton et al., 2006; Shehata et al., 2012; Sleeman et al., 2005; Stingl et al., 2006). Independent tumors were dissociated to single-cell suspensions and stained for CD24, CD29, CD49f, and EpCAM cell-surface markers. Tumors displayed distinct FACS profiles showing heterogeneous expression for different markers but with enrichment for CD24$^+$CD29$^+$ and CD24$^+$EpCAM$^+$ cell subsets (Figures 1D and S1D). The GFP$^+$ cell population was homogeneous, with the majority of cells being located in the Lin$^-$CD24$^+$ cell subset and expressing CD29, CD49f, and EpCAM cell-surface markers (Figure 1D). Moreover, Lin$^-$GFP$^+$ cells showed a higher percentage of double-positive [CD24 CD49f]$^+$ in comparison with total Lin$^-$ tumor cells (Figure S1D).

Figure 1. s-SHIP/GFP Expression Is Detected in Mammary Tumors of s-SHIP-GFP/C3(1)-Tag Bitransgenic Mice

(A) H&E staining of paraffin-embedded sections of mammary tumors illustrating different stages of tumor development: a, ductal hyperplasia; b, ductal carcinoma *in situ*; c, infiltrative solid carcinoma; d, solid carcinoma. Scale bars, 50 μm (a, b, d) and100 μm (c). See also Figure S1A.

(B) Representative images (n = 4) of frozen sections of mammary tumors containing GFP$^+$ cells (green) and stained with cytokeratin 14 (K14, red, upper panels), cytokeratin 8 (K8, red, lower panels), and DAPI nuclear stain (blue) Scale bars, 100 μm (left panels) and 10 μm (right panels). Images of 7-week-old mammary gland stained with K14 and K8 are shown in Figure S1B.

(C) Representative flow cytometry analysis (n = 5) of GFP expression in dissociated mammary cancer cells isolated from a 5-month-old bitransgenic mouse. P1 gate is set as to exclude dead cells (Zombie violet$^+$). See also Figure S1C.

(D) Representative flow cytometry analysis (n = 3) of total Lin$^-$ cells, Lin$^-$GFP$^-$, and Lin$^-$GFP$^+$ cells from two different tumors: T1 and T2. Cells were analyzed for the expression of CD24, CD29, CD49f, and EpCAM cell-surface markers. See also Figure S1D.

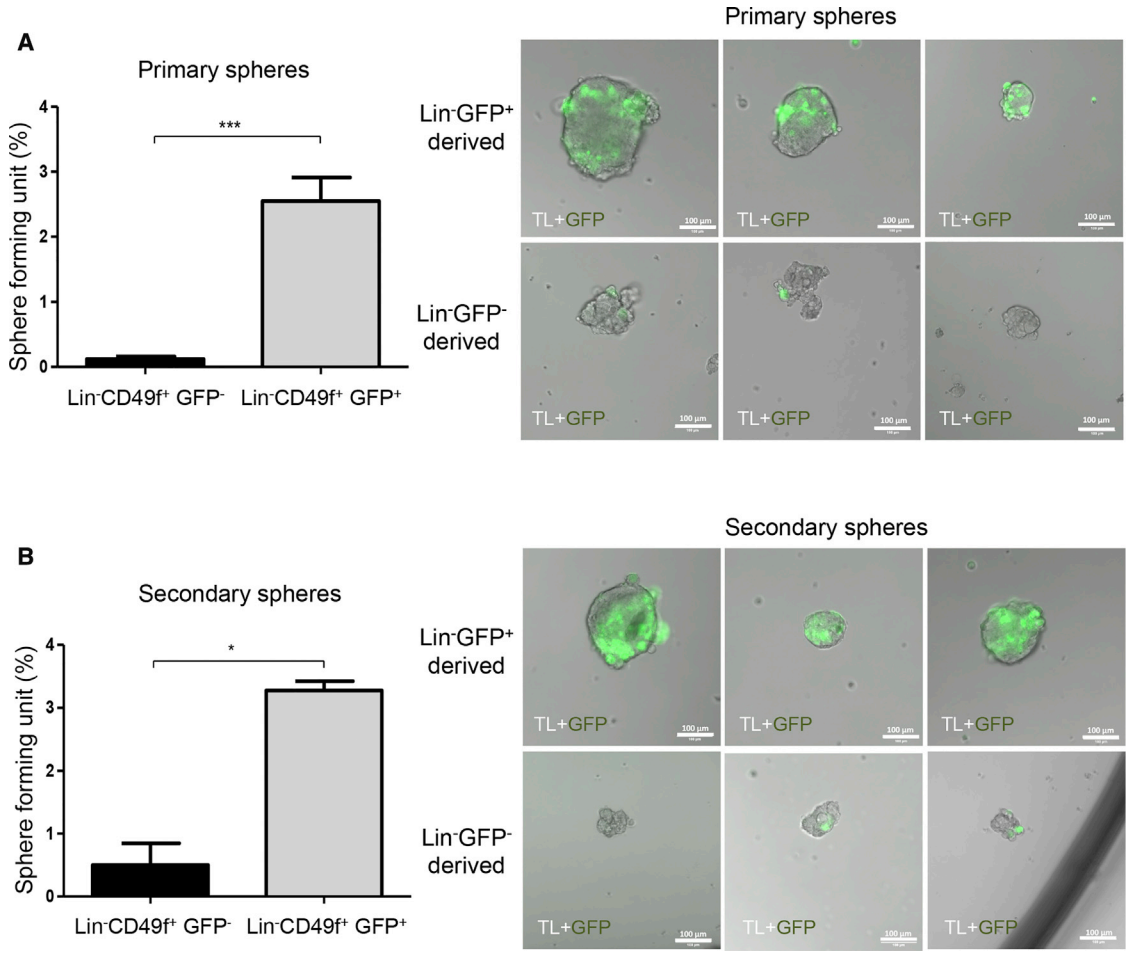

Figure 2. s-SHIP/GFP$^+$ Cells Have Higher Sphere-Forming Potential and *In Vitro* Self-Renewal Capacity

(A) Primary mammospheres derived from Lin$^-$CD49f$^+$GFP$^-$ and Lin$^-$CD49f$^+$GFP$^+$ cells isolated from bitransgenic mammary tumors. Cells were seeded by limited dilution and grown in suspension for 7–10 days. Data represent the mean ± SEM of seven independent experiments; p values were determined by Student's t test, ***p < 0.001. Right panels: representative pictures of primary spheres after 7–10 days of culture.

(B) Primary spheres derived from Lin$^-$CD49f$^+$GFP$^-$ or Lin$^-$CD49f$^+$GFP$^+$ cells were dissociated into single cells. Cells were seeded at 200 cells per well in triplicate and grown in suspension for 7–10 days for secondary mammosphere formation. Data represent mean ± SEM of three different experiments; p values were determined by Student's t test, *p < 0.05. Right panels: representative pictures of secondary spheres after 7–10 days of culture.

Scale bars, 100 μm. See also Figures S2A and S2B for cell-sorting strategy and experimental design, and Figure S3A.

s-SHIP/GFP$^+$ Tumor Cells Are Enriched for Sphere-Forming and Tumorigenic Cells

To further characterize GFP$^+$ cells, we used CD49f expression to separate GFP$^+$ epithelial cells (CD49f^{high}) from the few GFP$^+$ vascular smooth muscle cells (CD49f$^{-/low}$) as previously reported (Bai and Rohrschneider, 2010) (Figure S2A). To compare the frequency of TICs in GFP$^+$ versus GFP$^-$ cell subsets we isolated cells by FACS, and either cultured them under serum-free suspension conditions to form mammospheres or subcutaneously injected them into SCID mice (Figure S2B). Since the majority of GFP$^+$ cells were located in the Lin$^-$ cell fraction, we compared Lin$^-$CD49f$^+$GFP$^+$ cells with Lin$^-$CD49f$^+$GFP$^-$ cells (Figure S2B). GFP$^+$ cell populations showed a significant higher sphere-forming potential (2.55% ± 1.92%) compared with the control GFP$^-$ cell populations (0.12% ± 0.22%) (Figure 2A, left panel, n = 7). Spheres derived from GFP$^+$ cells were heterogeneous in size but most often larger compared with those derived from GFP$^-$ cells (Figure 2A, right panels). To examine the *in vitro* self-renewal potential of GFP$^+$ cells, we dissociated primary spheres into single-cell suspensions and plated the cells under the same conditions as for primary spheres. Secondary spheres derived from GFP$^+$ subgroups were more numerous and larger as

A

Primary injection in SCID mice

	1000 cells	100 cells	50 cells	Tumor initiating cell frequency (95% CI)
Lin$^-$ CD49f$^+$ GFP$^-$	5/6	3/22	1/17	**1/638** (1/1257 - 1/324)
Lin$^-$ CD49f$^+$ GFP$^+$	6/6	10/22	9/17	**1/118** (1/188 - 1/74)

P=2.65^{e-05}

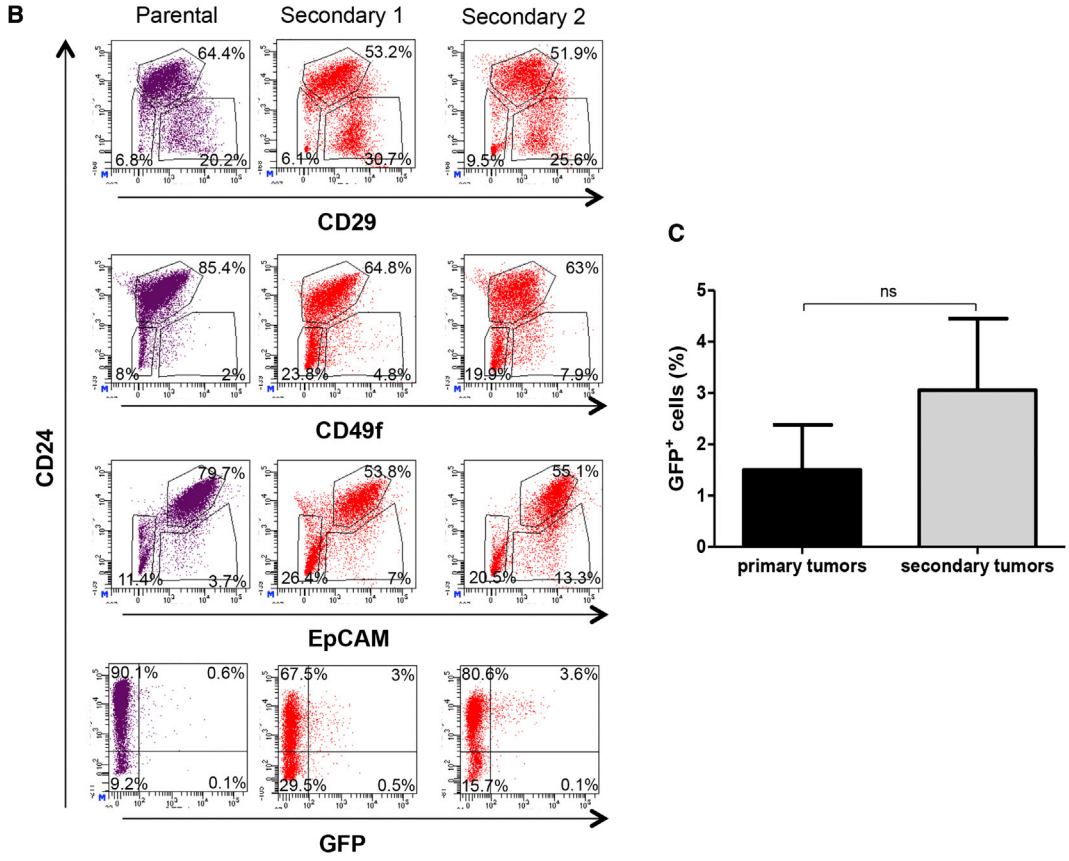

D

Secondary injection in SCID mice

	1000 cells	100 cells	50 cells	Tumor initiating cell frequency (95% CI)
Lin$^-$ CD49f$^+$ GFP$^-$	4/4	6/11	2/11	**1/157** (1/311 - 1/80)
Lin$^-$ CD49f$^+$ GFP$^+$	4/4	11/11	10/11	**1/20** (1/40 - 1/10)

P=5.32^{e-06}

Figure 3. s-SHIP/GFP$^+$ Cells Are Enriched for Tumor-Initiating Cells and Generate Tumors that Mimic the Parental Tumors

(A) Flow cytometry was used to separate dissociated tumor cells based on cell-surface markers and GFP expression (see Figure S2B for experimental procedures). The collected cell populations were injected subcutaneously into recipient SCID female mice in a limiting dilution manner. Mice were monitored until tumors were observed or up to 7 months if no tumors were detected. See also Figures S2C, S2D, and S3B.

(legend continued on next page)

compared with secondary spheres derived from GFP$^-$ subgroups (Figure 2B, n = 3). Spheres initially derived from GFP$^+$ cell subsets can be maintained through at least four passages (data not shown). It is noteworthy that few GFP$^+$ cells were always observed in the spheres at all passages (Figures 2 and S3A).

We next performed serial transplantation studies to evaluate the tumorigenic potential of GFP$^+$ cells versus GFP$^-$ cells and to determine whether GFP$^+$ cells were able to self-renew *in vivo* and recapitulate the cell heterogeneity of the original tumors. When injected subcutaneously in the region next to the nipple of the third thoracic gland of immunodeficient SCID mice, GFP$^+$ cells displayed significantly higher tumorigenic potential compared with GFP$^-$ cells (Figure 3A). The calculated TIC frequency in the Lin$^-$CD49f$^+$GFP$^-$ cell population was 1 in 638 tumor cells whereas it was of 1 in 118 in the Lin$^-$CD49f$^+$GFP$^+$ cell population. No difference was observed in tumor latency (Figure S3B). Similar TIC frequency was observed in CD49f$^+$GFP$^+$ without lineage depletion (Figure S2C). For CD49f$^+$GFP$^-$ cells, TIC frequency was lower compared with Lin$^-$CD49f$^+$GFP$^-$ cells. This could be explained by a dilution effect of numerous Lin$^+$ cells present in the tumor, but also may indicate an inhibitory effect of some Lin$^+$ cells on tumorigenicity. C3(1)-Tag mammary tumor cells and tumor-derived cell lines cannot be transplanted into immunocompetent FVB mice, since they are rejected likely due to the expression of the SV40 T antigen (Aprelikova et al., 2016). However, we have successfully transplanted primary tumor cells into FVB mice but with a significantly lower engraftment rate as well as longer tumor-formation period (4–7 months) compared with SCID mice (1–3 months, Figure S3B). Nevertheless, Lin$^-$CD49f$^+$GFP$^+$ cells were again capable of generating more tumors than Lin$^-$CD49f$^+$GFP$^-$ cells (Figure S2D).

Flow cytometry analysis of secondary tumors generated by Lin$^-$CD49f$^+$GFP$^+$ cells injected into SCID mice showed that the expression patterns of cell-surface markers were similar to those of the original tumor (Figure 3B). Interestingly, GFP$^+$ cells were also present in these secondary tumors (Figure 3B). The percentage of GFP$^+$ cells in secondary tumors was higher but not significantly different (Figure 3C). Transplantation experiments showed that both Lin$^-$CD49f$^+$GFP$^+$ and Lin$^-$CD49f$^+$GFP$^-$ cells isolated from these secondary tumors had higher tumor-forming capacities than their corresponding cell populations from primary tumors (Figures 3A and 3D). This suggests that both cell populations changed toward a more aggressive phenotype. Importantly, Lin$^-$CD49f$^+$GFP$^+$ cells still exhibited a higher tumorigenic potential in these secondary injections (1 in 20) compared with Lin$^-$CD49f$^+$GFP$^-$ cells (1 in 157) (Figure 3D).

Microarray Analysis Revealed DLK1 as a Negative Regulator of Stemness

To identify molecular differences between Lin$^-$CD49f$^+$GFP$^+$ and Lin$^-$CD49f$^+$GFP$^-$ cells, we performed transcriptional profiling using Agilent microarray technology. As shown in Figure 4A, Lin$^-$CD49f$^+$GFP$^+$ and Lin$^-$CD49f$^+$GFP$^-$ cell subpopulations shared a similar gene expression pattern (GEO accession number GEO: GSE108373). Nevertheless, microarray analysis revealed several genes whose expression differs significantly between the two subpopulations (Figure 4B) (Table S1). Granzyme E (GZME) was significantly upregulated in Lin$^-$CD49f$^+$GFP$^+$ cells (fold change of 29.8) (Figure 4B). Granzymes are a family of serine proteases expressed by immune cells (Arias et al., 2017). As a first approach, we delivered small interfering RNA (siRNA) to knock down *Gzme* expression in Lin$^-$CD49f$^+$GFP$^+$ cells and investigated the outcome of *Gzme* silencing on the sphere-forming potential of these cells. As shown in Figure S3C, the downregulation of *Gzme* did not affect the sphere-forming potential of GFP$^+$ cells. We were then interested in the Delta-like non-canonical Notch ligand 1 (*Dlk1*) gene that was significantly downregulated in Lin$^-$CD49f$^+$GFP$^+$ cells (fold change of 4.5) (Figure 4B). *Dlk1* gene encodes for a single-spanning transmembrane protein in the epidermal growth factor-like family, which includes NOTCH receptors and their ligands (Tanimizu et al., 2003). DLK1 is a non-canonical Notch ligand and has been shown to act as an inhibitor of Notch signaling *in vitro* (Nueda et al., 2017). Microarray analysis revealed the expression of *Notch1*, *Notch3*, and *Notch4* genes in Lin$^-$CD49f$^+$ cell populations. Chemical inhibition of NOTCH processing with the γ-secretase inhibitor Compound E decreased the sphere-forming potential of

(B) Secondary tumors derived from Lin$^-$CD49f$^+$GFP$^+$ cell fraction have flow-cytometric profiles similar to those of the primary tumors. Representative flow cytometry analysis of dissociated cells from a primary tumor (parental) and two respective secondary tumors (secondary 1 and 2) are presented.

(C) The percentage of Lin$^-$CD49f$^+$GFP$^+$ cells in secondary tumors and corresponding primary parental tumors. Data represent mean values ± SEM of four different experiments; p values were determined by Student's t test, not significant (ns).

(D) Cells from secondary tumors generated by Lin$^-$CD49f$^+$GFP$^+$ fraction were freshly digested and FACS sorted into Lin$^-$CD49f$^+$GFP$^-$ or Lin$^-$CD49f$^+$GFP$^+$ subpopulations, and injected into SCID mice as described in (A).

In (A) and (D), tumor-initiating cell frequencies and p values were generated by extreme limiting dilution analysis (ELDA). See also Figures S2A and S2B for cell-sorting strategy and experimental design.

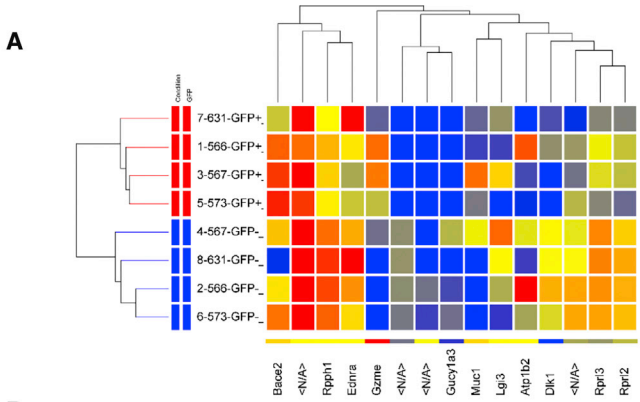

B

GeneSymbol	Description	p	Regulation	FC (abs)
Gzme	granzyme E	**0.00991789**	up	29.83715
Dlk1	delta-like 1 homolog (Drosophila)	**0.00414383**	down	4.5239267
Gucy1a3	guanylate cyclase 1, soluble, alpha 3	**0.00643437**	down	4.0955086
	Mus musculus cDNA clone IMAGE:40090117, [BC128469]	**0.00405105**	down	3.5768538
Rprl3	ribonuclease P RNA-like 3	**0.00658998**	down	3.2771783
	lincRNA:chr13:22110479-22116629 reverse strand	**0.00622081**	down	3.1527982
Rprl2	ribonuclease P RNA-like 2	**0.00696632**	down	2.9873924
Rpl7	ribosomal protein L7A	**0.00653786**	down	2.50248
Rpph1	ribonuclease P RNA component H1	**0.00963502**	down	2.4559698
Bace2	beta-site APP-cleaving enzyme 2	**0.00738185**	up	2.404046
Muc1	mucin 1, transmembrane	**0.00493007**	up	2.170539
Atp1b2	ATPase, Na+/K+ transporting, beta 2 polypeptide	**0.00842456**	down	2.1331136
Ednra	endothelin receptor type A	**0.00942573**	down	2.0767322
	lincRNA:chr6:47687025-47728525 forward strand	**0.00465488**	down	2.0415895
Lgi3	10 days neonate medulla oblongata cDNA, RIKEN full-length enriched library, clone:B830040F02 product:leucine-rich repeat LGI family, member 3, full insert sequence, [AK163664]	**3.07E-06**	down	2.016158

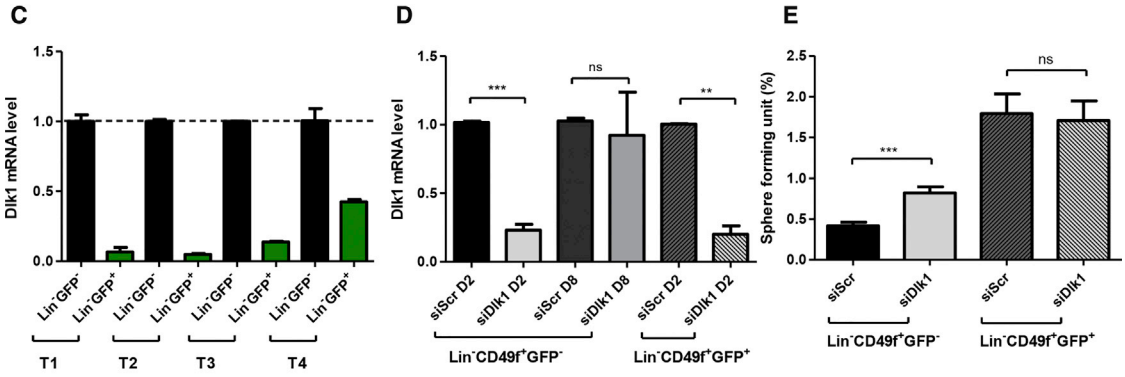

F

	600 cells	300 cells	100 cells	Tumor initiating cell frequency (95% CI)
Lin$^-$CD49f$^+$GFP$^-$ siScr	13/28	7/28	5/20	**1/859** (1/1283 – 1/575)
Lin$^-$CD49f$^+$GFP$^-$ siDlk1	20/28	21/28	5/20	**1/340** (1/467 – 1/248)

P=2.09^{e-04}

Figure 4. Gene Expression Analysis of Lin$^-$CD49f$^+$GFP$^-$ versus Lin$^-$CD49f$^+$GFP$^+$ Tumor Cells Reveals the Role of DLK1 in the Regulation of Stemness

(A and B) Fifteen genes (B) were selected from the master list of genes differentially regulated (at least 2-fold with a p value <0.05). A list of 355 deregulated probes (fold change $\geq$1) is presented in Table S1. For the heatmap (A), each column represents a probe; each row

(legend continued on next page)

Lin$^-$CD49f$^+$GFP$^+$ cells (Figure S3D). Thus, we hypothesized that repression of the Notch-negative regulator DLK1 in Lin$^-$CD49f$^+$GFP$^+$ cells might favor their CSC phenotype. The difference in *Dlk1* expression between Lin$^-$CD49f$^+$GFP$^-$ and Lin$^-$CD49f$^+$GFP$^+$ subpopulations was first confirmed by qRT-PCR using total RNA isolated from these two subpopulations. Similar to microarray results, we observed a fold change of 11 ± 8 (Figure 4C, n = 4 different tumors). We thus delivered siRNA to knock down *Dlk1* expression in Lin$^-$CD49f$^+$GFP$^-$ cells and performed sphere-forming assays. Lin$^-$CD49f$^+$GFP$^-$ cell subpopulation was transfected with si*Dlk1* or siScramble (siScr) and then cultured in serum-free sphere medium under non-adherent conditions for 7–10 days. A transient downregulation of *Dlk1* expression was obtained with 77% of inhibition after 2 days of culture, and only 10% of inhibition in the generated spheres at day 8 (Figure 4D). We observed a significant increase of the sphere-forming potential of si*Dlk1*-treated cells (0.82% ± 0.21%) compared with siScr-treated cells (0.42% ± 0.12%) (Figure 4E). On the contrary, a downregulation of 80% of *Dlk1* expression in Lin$^-$CD49f$^+$GFP$^+$ cells (Figure 4D) did not interfere with their sphere-forming potential (Figure 4E), suggesting that the level of *Dlk1* expression in these cells may be too low to have any inhibitory effect on their sphere-forming capacity. Since si*Dlk1* enhanced the *in vitro* sphere-forming potential of Lin$^-$CD49f$^+$GFP$^-$ cells, we next performed transplantation studies to evaluate the tumorigenic potential of si*Dlk1*- and siScr-transfected Lin$^-$CD49f$^+$GFP$^-$ cells. The calculated TIC frequency in the si*Dlk1*-transfected Lin$^-$CD49f$^+$GFP$^-$ cell population was 1 in 340 tumor cells whereas it was 1 in 859 in the si*Scr*-transfected Lin$^-$CD49f$^+$GFP$^-$ cells (Figure 4F). No difference was observed in the tumor latency (Figure S3E). Thus, downregulation of *Dlk1* in Lin$^-$CD49f$^+$GFP$^-$ cells significantly increased both their sphere-forming potential *in vitro* and their tumorigenic potential *in vivo* compared with control cells. Altogether, these results suggest that DLK1 could act as a negative regulator of stemness of mammary cancer cells.

DISCUSSION

Stem cell-specific expression of s-SHIP was initially identified in hematopoietic and embryonic stem cells (Rohrschneider et al., 2005; Tu et al., 2001). Using s-SHIP-GFP promoter reporter, its stem cell-specific expression has been demonstrated in prostate tissues (Al Shareef et al., 2018; Bauderlique-Le Roy et al., 2015; Brocqueville et al., 2016). In postnatal mammary gland development, GFP$^+$ cap cells in puberty and basal alveolar bud cells in pregnancy each exhibit stem cell properties (Bai and Rohrschneider, 2010). In the same study, the authors described the presence of GFP$^+$ tumor cells in heterogeneous luminal/basal-like mammary tumors originating in bitransgenic s-SHIP-GFP/MMTV-Wnt1 mice. Subsequent studies have demonstrated the value of s-SHIP promoter to investigate normal mammary stem cells (Huo and Macara, 2014; Kogata et al., 2013; Roarty et al., 2015). However, s-SHIP/GFP usefulness in isolating mammary CSCs remains to be determined. Here we used a mouse model of basal-like breast cancer to show that s-SHIP is a marker of mammary CSCs. In our s-SHIP-GFP/C3(1)-Tag bitransgenic mice, s-SHIP/GFP$^+$ cells expressed commonly used mammary CSC cell-surface markers, exhibited a higher sphere-forming potential *in vitro*, and a higher ability to reform secondary tumors when transplanted into recipient mice. Interestingly, transplanted s-SHIP/GFP$^+$ cells generated heterogeneous tumors that displayed properties similar to those of the primary tumors, including the presence of a subset of s-SHIP/GFP$^+$ cells with CSC properties. Bai and Rohrschneider (2010) did not observe s-SHIP/GFP$^+$ cells in tumors of bitransgenic s-SHIP-GFP/MMTV-ErbB2/neu/HER2 mice exhibiting luminal features. Considering breast CSC heterogeneity, it remains to be determined whether s-SHIP expression is restricted or not to CSCs in basal-like breast cancer. To address this question, we aim to characterize the exact nature of s-SHIP/GFP$^+$ tumor cells that have been observed in heterogeneous mammary tumors developed by bitransgenic s-SHIP-GFP/MMTV-Wnt1 mice

represents various subpopulations from biological replicates. The red color indicates high-level expression while blue indicates a low level of expression.

(C) qRT-PCR confirmed the downregulation of *Dlk1* expression in Lin$^-$CD49f$^+$GFP$^+$ cells compared with Lin$^-$CD49f$^+$GFP$^-$ cells. Data represent mean values ± SEM from four different tumors (T1 to T4).

(D and E) Inhibition of *Dlk1* expression in Lin$^-$CD49f$^+$GFP$^-$ cells increased their sphere-forming potential. si*Dlk1* or control siScramble (siScr) were introduced into Lin$^-$CD49f$^+$GFP$^-$ and Lin$^-$CD49f$^+$GFP$^+$ cells isolated from bitransgenic mammary tumors. (D) The level of *Dlk1* mRNA was determined by qRT-PCR, 2 days or 8 days after siRNA transfection. (E) Lin$^-$CD49f$^+$GFP$^-$ and Lin$^-$CD49f$^+$GFP$^+$ cells were treated by siScr or si*Dlk1*, and plated under sphere conditions. Spheres were counted after 7–10 days in culture. Data represent mean values ± SEM of six independent experiments; p values were determined by Student's t test, ***p < 0.001 **p < 0.01; ns, not significant. See Figures S3C and S3D for additional experiments.

(F) siScr or si*Dlk1* transfected Lin$^-$CD49f$^+$GFP$^-$ cells were injected subcutaneously into recipient SCID female mice in a limiting dilution manner. Mice were monitored until tumors were observed or up to 3 months if no tumors were detected. Tumor-initiating cell frequencies and p values were generated by ELDA. See also Figure S3E.

(Bai and Rohrschneider, 2010), together with an in-depth analysis of data for breast cancer from The Cancer Genome Atlas.

Transcriptional profiling showed few genes differentially expressed between Lin$^-$CD49f$^+$GFP$^+$ and Lin$^-$CD49f$^+$GFP$^-$ cells. Among them, the significant decrease of *Dlk1* expression in GFP$^+$ cells has attracted our attention. DLK1 acts as a non-canonical ligand of the Notch signaling pathway and is expressed at a high frequency in various human tumors including breast carcinoma (Yanai et al., 2010). Several studies have demonstrated that DLK1 can act as an inhibitor of Notch signaling *in vitro*, including in breast cancer cells (Nueda et al., 2017). Our results strongly suggest that DLK1 acts as a negative regulator of stemness in breast cancer, which agrees with several studies pointing to a role of Notch pathway in breast cancer, especially in subtypes with stem-like features and endothelial-to-mesenchymal transition (Harrison et al., 2010). Based on our results, we can hypothesize that DLK1 interacts with Notch receptor expressed by tumor cells and can act as a negative regulator of Notch activation and signaling in these tumors cells. It is likewise possible that DLK1 action implicates cells of the tumor microenvironment. Interestingly, a recent study showed that Notch ligand Dll1 mediates crosstalk between mammary stem cells and tissue-resident macrophages (Chakrabarti et al., 2018). This implies that DLK1 may also be involved in the modulation of the oncogenic potential of mammary tumor cells through the inhibition of Notch signaling in surrounding macrophages. To address this issue, it would be important to determine the relationship between breast CSCs, macrophages, DLK1, and Notch signaling.

Taken together, our results strongly support the relationship between mammary CSCs and s-SHIP expression. This is in accordance with high s-SHIP expression in murine claudin-low tumors that are enriched for CSC signature (Herschkowitz et al., 2012). s-SHIP protein is a shorter isoform of SHIP1 protein that lacks the SH2 domain in its N-terminal region (Tu et al., 2001). However, the function of s-SHIP protein remains unknown. SHIP2, the ubiquitous homolog of SHIP1, is crucial for maintaining the ER-negative breast CSCs through activation of Akt and JNK (Fu et al., 2014). Since our data indicate s-SHIP as a potential clinical target for breast cancer therapy, the expression and role of s-SHIP in human breast cancers will be the subject of our future investigation.

EXPERIMENTAL PROCEDURES

All animal procedures were performed under a protocol (#01989.02) approved by the Animal Protocol Review Committees of the Institut Pasteur de Lille (France) in accordance with European regulation.

Statistics

Data are expressed as means ± SEM of at least three independent experiments. The statistical analysis was done by using two-way ANOVA or Student's t test with GraphPad Prism5, and a p value of <0.05 was considered significant. For *in vivo* tumor-initiating potential, the results were analyzed by extreme limiting dilution analysis (ELDA) (Hu and Smyth, 2009).

ACCESSION NUMBERS

The accession number for the microarray dataset reported in this paper is GEO: GSE108373.

SUPPLEMENTAL INFORMATION

Supplemental Information can be found online at https://doi.org/10.1016/j.stemcr.2019.05.013.

AUTHOR CONTRIBUTIONS

M-J. T. and C.L. contributed equally to this work. L.T., M.-J.T., E.B., H.B.-L.R., M.F., and R.P.B. did the experiments L.T., C.L., E.A., X.L.B., and R.P.B. designed the study. L.T. and R.P.B. wrote the main manuscript text, and all authors reviewed the manuscript.

ACKNOWLEDGMENTS

We thank S. Sebda and F. Leprêtre (Functional Genomic Platform, Lille) for microarrays hybridization and for GEO repository assistance, Q. Pascal (OCR, Loos) for anatomopathological analysis, and S. Salomé-Desnoulez (BICel), M.-C. Bouchez (CNRS), and T. Chassat (IPL) for their help. This study was supported by grants from the SIRIC ONCOLille (INCa-DGOS-Inserm 6041), the Ligue Contre le Cancer (comités du Nord et du Pas-de-Calais), and the Cancéropole Nord-Ouest. L.T. was supported by fellowships from the Région Hauts-de-France and the Fondation ARC pour la Recherche sur le Cancer.

Received: July 10, 2018
Revised: May 13, 2019
Accepted: May 14, 2019
Published: June 13, 2019

REFERENCES

Al-Hajj, M., Wicha, M.S., Benito-Hernandez, A., Morrison, S.J., and Clarke, M.F. (2003). Prospective identification of tumorigenic breast cancer cells. Proc. Natl. Acad. Sci. U S A *100*, 3983–3988.

Al Shareef, Z., Kardooni, H., Murillo-Garzón, V., Domenici, G., Stylianakis, E., Steel, J.H., Rabano, M., Gorroño-Etxebarria, I., Zabalza, I., Vivanco, M.D., et al. (2018). Protective effect of stromal dickkopf-3 in prostate cancer: opposing roles for TGFBI and ECM-1. Oncogene *37*, 5305–5324.

Aprelikova, O., Tomlinson, C.C., Hoenerhoff, M., Hixon, J.A., Durum, S.K., Qiu, T., He, S., Burkett, S., Liu, Z.-Y., Swanson, S.M., et al. (2016). Development and preclinical application of an immunocompetent transplant model of basal breast cancer with lung, liver and brain metastases. PLoS One *11*, e0155262.

Arias, M., Martinez-Lostao, L., Santiago, L., Ferrandez, A., Granville, D.J., and Pardo, J. (2017). The untold story of granzymes in oncoimmunology: novel opportunities with old acquaintances. Trends Cancer *3*, 407–422.

Bai, L., and Rohrschneider, L.R. (2010). s-SHIP promoter expression marks activated stem cells in developing mouse mammary tissue. Genes Dev. *24*, 1882–1892.

Bauderlique-Le Roy, H., Vennin, C., Brocqueville, G., Spruyt, N., Adriaenssens, E., and Bourette, R.P. (2015). Enrichment of human stem-like prostate cells with s-SHIP promoter activity uncovers a role in stemness for the long noncoding RNA H19. Stem Cells Dev. *24*, 1252–1262.

Brocqueville, G., Chmelar, R.S., Bauderlique-Le Roy, H., Deruy, E., Tian, L., Vessella, R.L., Greenberg, N.M., Rohrschneider, L.R., and Bourette, R.P. (2016). s-SHIP expression identifies a subset of murine basal prostate cells as neonatal stem cells. Oncotarget *7*, 29228–29244.

Brooks, M.D., Burness, M.L., and Wicha, M.S. (2015). Therapeutic implications of cellular heterogeneity and plasticity in breast cancer. Cell Stem Cell *17*, 260–271.

Chakrabarti, R., Celià-Terrassa, T., Kumar, S., Hang, X., Wei, Y., Choudhury, A., Hwang, J., Peng, J., Nixon, B., Grady, J.J., et al. (2018). Notch ligand Dll1 mediates cross-talk between mammary stem cells and the macrophageal niche. Science *360*, eaan4153.

Cho, R.W., Wang, X., Diehn, M., Shedden, K., Chen, G.Y., Sherlock, G., Gurney, A., Lewicki, J., and Clarke, M.F. (2008). Isolation and molecular characterization of cancer stem cells in MMTV-Wnt-1 murine breast tumors. Stem Cells *26*, 364–371.

Dontu, G., and Ince, T.A. (2015). Of mice and women: a comparative tissue biology perspective of breast stem cells and differentiation. J. Mammary Gland Biol. Neoplasia *20*, 51–62.

Fu, C.-H., Lin, R.-J., Yu, J., Chang, W.-W., Liao, G.-S., Chang, W.-Y., Tseng, L.-M., Tsai, Y.-F., Yu, J.-C., and Yu, A.L. (2014). A novel oncogenic role of inositol phosphatase SHIP2 in ER-negative breast cancer stem cells: involvement of JNK/vimentin activation. Stem Cells *32*, 2048–2060.

Ginestier, C., Hur, M.H., Charafe-Jauffret, E., Monville, F., Dutcher, J., Brown, M., Jacquemier, J., Viens, P., Kleer, C.G., Liu, S., et al. (2007). ALDH1 is a marker of normal and malignant human mammary stem cells and a predictor of poor clinical outcome. Cell Stem Cell *1*, 555–567.

Gusterson, B., and Eaves, C.J. (2018). Basal-like breast cancers: from pathology to biology and back again. Stem Cell Reports *10*, 1676–1686.

Harrison, H., Farnie, G., Brennan, K.R., and Clarke, R.B. (2010). Breast cancer stem cells: something out of notching? Cancer Res. *70*, 8973–8976.

Herschkowitz, J.I., Simin, K., Weigman, V.J., Mikaelian, I., Usary, J., Hu, Z., Rasmussen, K.E., Jones, L.P., Assefnia, S., Chandrasekharan, S., et al. (2007). Identification of conserved gene expression features between murine mammary carcinoma models and human breast tumors. Genome Biol. *8*, R76.

Herschkowitz, J.I., Zhao, W., Zhang, M., Usary, J., Murrow, G., Edwards, D., Knezevic, J., Greene, S.B., Darr, D., Troester, M.A., et al. (2012). Comparative oncogenomics identifies breast tumors enriched in functional tumor-initiating cells. Proc. Natl. Acad. Sci. U S A *109*, 2778–2783.

Hu, Y., and Smyth, G.K. (2009). ELDA: extreme limiting dilution analysis for comparing depleted and enriched populations in stem cell and other assays. J. Immunol. Methods *347*, 70–78.

Huo, Y., and Macara, I.G. (2014). The Par3-like polarity protein Par3L is essential for mammary stem cell maintenance. Nat. Cell Biol. *16*, 526–534.

Kogata, N., Zvelebil, M., and Howard, B.A. (2013). Neuregulin 3 and Erbb signalling networks in embryonic mammary gland development. J. Mammary Gland Biol. Neoplasia *18*, 149–154.

Maroulakou, I.G., Anver, M., Garrett, L., and Green, J.E. (1994). Prostate and mammary adenocarcinoma in transgenic mice carrying a rat C3(1) simian virus 40 large tumor antigen fusion gene. Proc. Natl. Acad. Sci. U S A *91*, 11236–11240.

Medema, J.P. (2013). Cancer stem cells: the challenges ahead. Nat. Cell Biol. *15*, 338–344.

Menezes, M.E., Das, S.K., Emdad, L., Windle, J.J., Wang, X.Y., Sarkar, D., and Fisher, P.B. (2014). Genetically engineered mice as experimental tools to dissect the critical events in breast cancer. Adv. Cancer Res. *121*, 331–382.

Nassar, D., and Blanpain, C. (2016). Cancer stem cells: basic concepts and therapeutic implications. Annu. Rev. Pathol. *11*, 47–76.

Nueda, M.L., Naranjo, A.I., Baladrón, V., and Laborda, J. (2017). Different expression levels of DLK1 inversely modulate the oncogenic potential of human MDA-MB-231 breast cancer cells through inhibition of NOTCH1 signaling. FASEB J. *31*, 3484–3496.

Peitzsch, C., Tyutyunnykova, A., Pantel, K., and Dubrovska, A. (2017). Cancer stem cells: the root of tumor recurrence and metastases. Semin. Cancer Biol. *44*, 10–24.

Pfefferle, A.D., Herschkowitz, J.I., Usary, J., Harrell, J.C., Spike, B.T., Adams, J.R., Torres-Arzayus, M.I., Brown, M., Egan, S.E., Wahl, G.M., et al. (2013). Transcriptomic classification of genetically engineered mouse models of breast cancer identifies human subtype counterparts. Genome Biol. *14*, R125.

Roarty, K., Shore, A.N., Creighton, C.J., and Rosen, J.M. (2015). Ror2 regulates branching, differentiation, and actin-cytoskeletal dynamics within the mammary epithelium. J. Cell Biol. *208*, 351–366.

Rohrschneider, L.R., Custodio, J.M., Anderson, T.A., Miller, C.P., and Gu, H. (2005). The intron 5/6 promoter region of the *ship1* gene regulates expression in stem/progenitor cells of the mouse embryo. Dev. Biol. *283*, 503–521.

Shackleton, M., Vaillant, F., Simpson, K.J., Stingl, J., Smyth, G.K., Asselin-Labat, M.L., Wu, L., Lindeman, G.J., and Visvader, J.E. (2006). Generation of a functional mammary gland from a single stem cell. Nature *439*, 84–88.

Shafee, N., Smith, C.R., Wei, S., Kim, Y., Mills, G.B., Hortobagyi, G.N., Stanbridge, E.J., and Lee, E.Y. (2008). Cancer stem cells contribute to cisplatin resistance in Brca1/p53–mediated mouse mammary tumors. Cancer Res. *68*, 3243–3250.

Shehata, M., Teschendorff, A., Sharp, G., Novcic, N., Russell, I.A., Avril, S., Prater, M., Eirew, P., Caldas, C., Watson, C.J., et al. (2012). Phenotypic and functional characterisation of the luminal cell hierarchy of the mammary gland. Breast Cancer Res. *14*, R134.

Sleeman, K.E., Kendrick, H., Ashworth, A., Isacke, C.M., and Smalley, M.J. (2005). CD24 staining of mouse mammary gland cells defines luminal epithelial, myoepithelial/basal and non-epithelial cells. Breast Cancer Res. *8*, R7.

Sreekumar, A., Roarty, K., and Rosen, J.M. (2015). The mammary stem cell hierarchy: a looking glass into heterogeneous breast cancer landscapes. Endocr. Relat. Cancer *22*, T161–T176.

Stingl, J., Eirew, P., Ricketson, I., Shackleton, M., Vaillant, F., Choi, D., Li, H.I., and Eaves, C.J. (2006). Purification and unique properties of mammary epithelial stem cells. Nature *439*, 993–997.

Tanimizu, N., Nishikawa, M., Saito, H., Tsujimura, T., and Miyajima, A. (2003). Isolation of hepatoblasts based on the expression of Dlk/Pref-1. J. Cell Sci. *116*, 1775–1786.

Torre, L.A., Bray, F., Siegel, R.L., Ferlay, J., Lortet-Tieulent, J., and Jemal, A. (2015). Global cancer statistics, 2012. CA Cancer J. Clin. *65*, 87–108.

Tu, Z., Ninos, J.M., Ma, Z., Wang, J.W., Lemos, M.P., Desponts, C., Ghansah, T., Howson, J.M., and Kerr, W.G. (2001). Embryonic and hematopoietic stem cells express a novel SH2–containing inositol 5′-phosphatase isoform that partners with the Grb2 adapter protein. Blood *98*, 2028–2038.

Usary, J., Darr, D.B., Pfefferle, A.D., and Perou, C.M. (2016). Overview of genetically engineered mouse model of distinct breast cancer subtypes. Curr. Protoc. Pharmacol. *72*, 14.38.1–14.38.11.

Vaillant, F., Asselin-Labat, M.-L., Shackleton, M., Forrest, N.C., Lindeman, G.J., and Visvader, J.E. (2008). The mammary progenitor marker CD61/β3 integrin identifies cancer stem cells in mouse models of mammary tumorigenesis. Cancer Res. *68*, 7711–7717.

Yanai, H., Nakamura, K., Hijioka, S., Kamei, A., Ikari, T., Ishikawa, Y., Shinozaki, E., Mizunuma, N., Hatake, K., and Miyajima, A. (2010). Dlk-1, a cell surface antigen on foetal hepatic stem/progenitor cells, is expressed in hepatocellular, colon, pancreas and breast carcinomas at a high frequency. J. Biochem. *148*, 85–92.

Zhang, M., Behbod, F., Atkinson, R.L., Landis, M.D., Kittrell, F., Edwards, D., Medina, D., Tsimelzon, A., Hilsenbeck, S., Green, J.E., et al. (2008). Identification of tumor-initiating cells in a p53 null mouse model of breast cancer. Cancer Res. *68*, 4674–4682.

Stem Cell Reports, Volume *13*

Supplemental Information

s-SHIP Promoter Expression Identifies Mouse Mammary Cancer Stem Cells

Lu Tian, Marie-José Truong, Chann Lagadec, Eric Adriaenssens, Emmanuel Bouchaert, Hélène Bauderlique-Le Roy, Martin Figeac, Xuefen Le Bourhis, and Roland P. Bourette

Figure S1

A

N° Animal	Type	Pattern	Infiltration	Stroma	Necrosis	Mitotic index	Peritumoral emboli
688	Carcinome	solid papillary with tubular carcinoma	2	1	3	150	2
796	Carcinome	solid papillary with tubular carcinoma	2	1	2	40	0
877	Carcinome	solid papillary with tubular carcinoma	3	1	1	104	3
921	Carcinome	solid papillary with tubular carcinoma	1	2	2	161	0
687	Carcinome	solid papillary with tubular carcinoma	3	2	2	86	1
766	Carcinome	tubulopapillary features	1	1	3	20	0
951	Carcinome	tubulopapillary features	2	1	2	77	2
978	Carcinome	tubulopapillary features	2	1	2	45	3
765	Carcinome	solide epithelial	1	1	1	81	3
808	Carcinome	solide epithelial	3	2	1	138	2
673	Carcinome	mixture of epithelial and spindle morphology	1	1	3	158	1
885	Carcinome	mixture of epithelial and spindle morphology	1	2	1	77	1
959	Carcinome	mixture of epithelial and spindle morphology	2	3	0	116	1
977	Carcinome	mixture of epithelial and spindle morphology	1	3	3	38	3

B

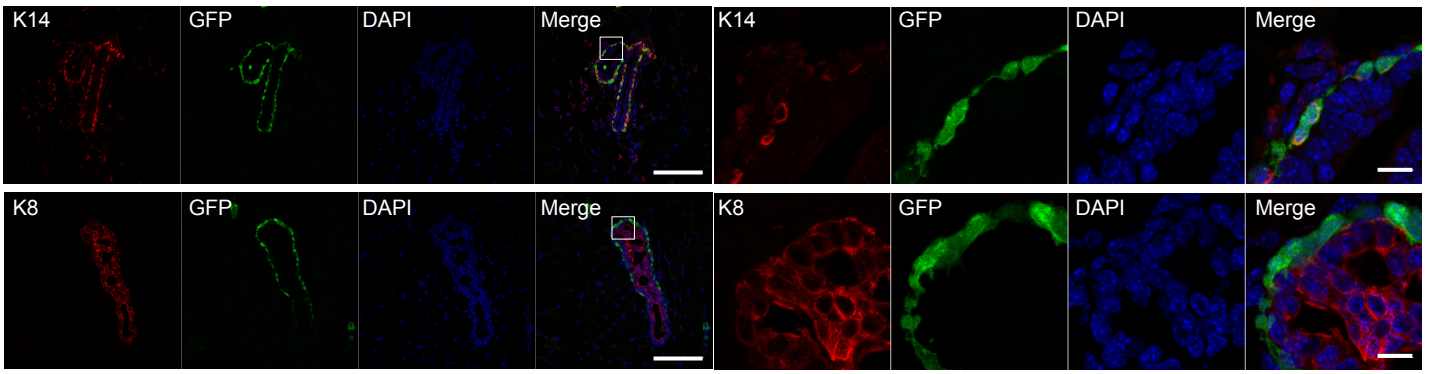

C

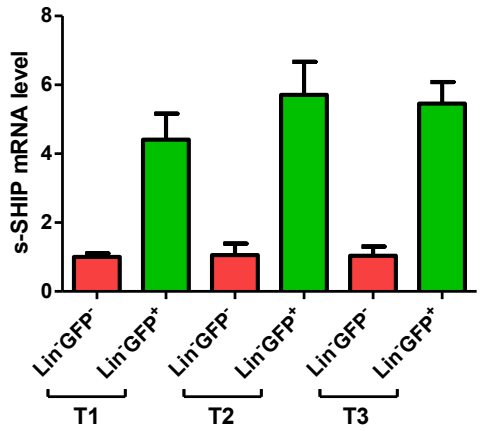

D

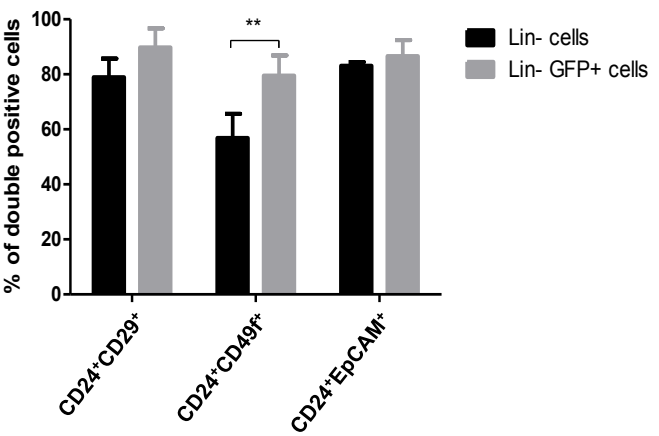

Figure S1. Analysis of mammary tumors from s-SHIP-GFP/C3(1)-Tag bi-transgenic mice. Related to Figure 1.
(**A**) Anatomopathological analysis of fourteen tumors isolated from 4 to 6-month-old bi-transgenic (biTg) mice.
(**B**) Representative photographs (n=3) of immunofluorescent staining for cytokeratin 14 (K14, upper panels), cytokeratin 8 (K8, lower panels) (red) and with DAPI nuclear stain (blue) of 7-week-old mammary gland of biTg mice containing GFP^+ cells (green) (scale bar = 100µm left panels and 10 µm right panels). (**C**) Expression level of endogenous s-SHIP mRNA was assessed from Lin^-GFP^- and Lin^-GFP^+ cell populations isolated from three different tumors (T1 to T3) using RT-qPCR.
(**D**) Flow cytometry analysis of CD24, CD29, CD49f and EpCAM cell surface marker expression on Lin^- cells and Lin^-GFP^+ cells. Data represent mean values ± SEM of three different tumors. *p* values were determined by Student's t-test $^{**}p < 0.01$.

Figure S2

A

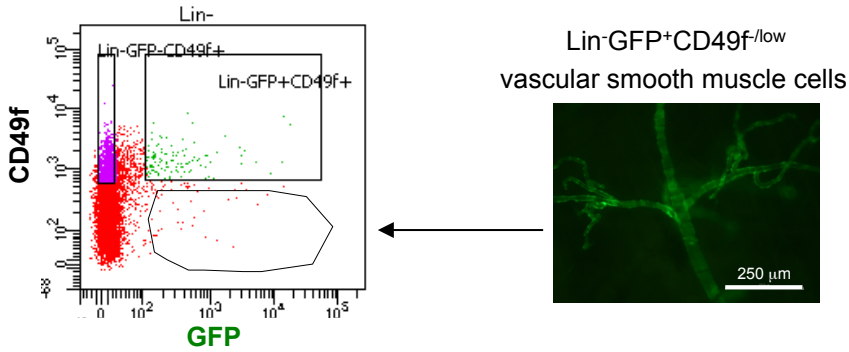

B

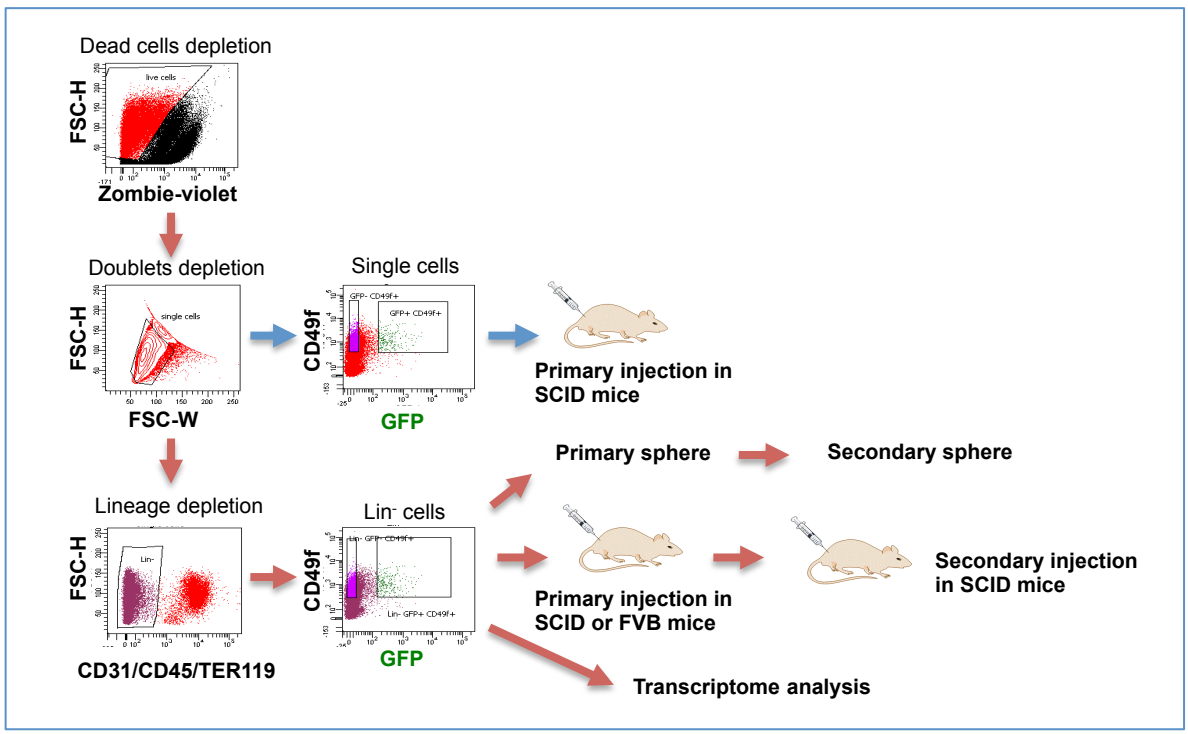

C

Primary injection in SCID mice without lineage depletion

	5000 cells	1000 cells	500 cells	100 cells	Tumor initiating cell frequency (95% CI)
CD49f$^+$ GFP$^-$	5/6	2/5	2/5	1/14	**1/2001** (1/4184 - 1/957)
CD49f$^+$ GFP$^+$	6/6	5/5	4/5	10/14	**1/129** (1/249 - 1/67)

P=2.25^{e-09}

D

Primary injection in FVB mice

	1000 cells	100 cells	Tumor initiating cell frequency (95% CI)
Lin$^-$ CD49f$^+$ GFP$^-$	1/11	1/14	**1/5918** (1/24165 - 1/1449)
Lin$^-$ CD49f$^+$ GFP$^+$	3/11	6/14	**1/1154** (1/2400 - 1/554)

P=0.0166

Figure S2. Experimental design for cell sorting and analysis of tumorigenic potential of s-SHIP/GFP$^+$ cells. Related to Figures 2, 3 and 4.

(**A**) Flow cytometry analysis showed a minor population of Lin$^-$ GFP$^+$ CD49$^{low/-}$ (left panel) corresponding to vascular smooth muscle cells (right panel) as previously described (Bai and Rohrschneider, 2010). Scale bar: 250 µm. (**B**) Cell sorting strategy and experimental design. FACS plot shows gates drawn for cell sorting of either CD49f$^+$GFP$^+$ and CD49$^+$GFP$^-$ cells, or Lin$^-$CD49f$^+$GFP$^+$ and Lin$^-$CD49f$^+$GFP$^-$ cells. (**C-E**) The collected cell populations were injected into recipient female mice in a limiting dilution manner. Mice were monitored until tumors were observed or up to 7 months if no tumors were detected. Tumor-initiating cell frequencies were generated by ELDA: extreme limiting dilution analysis. (**C**) Primary injection in immunodeficient SCID mice. (**D**) Primary injection in immunocompetent FVB mice.

Figure S3

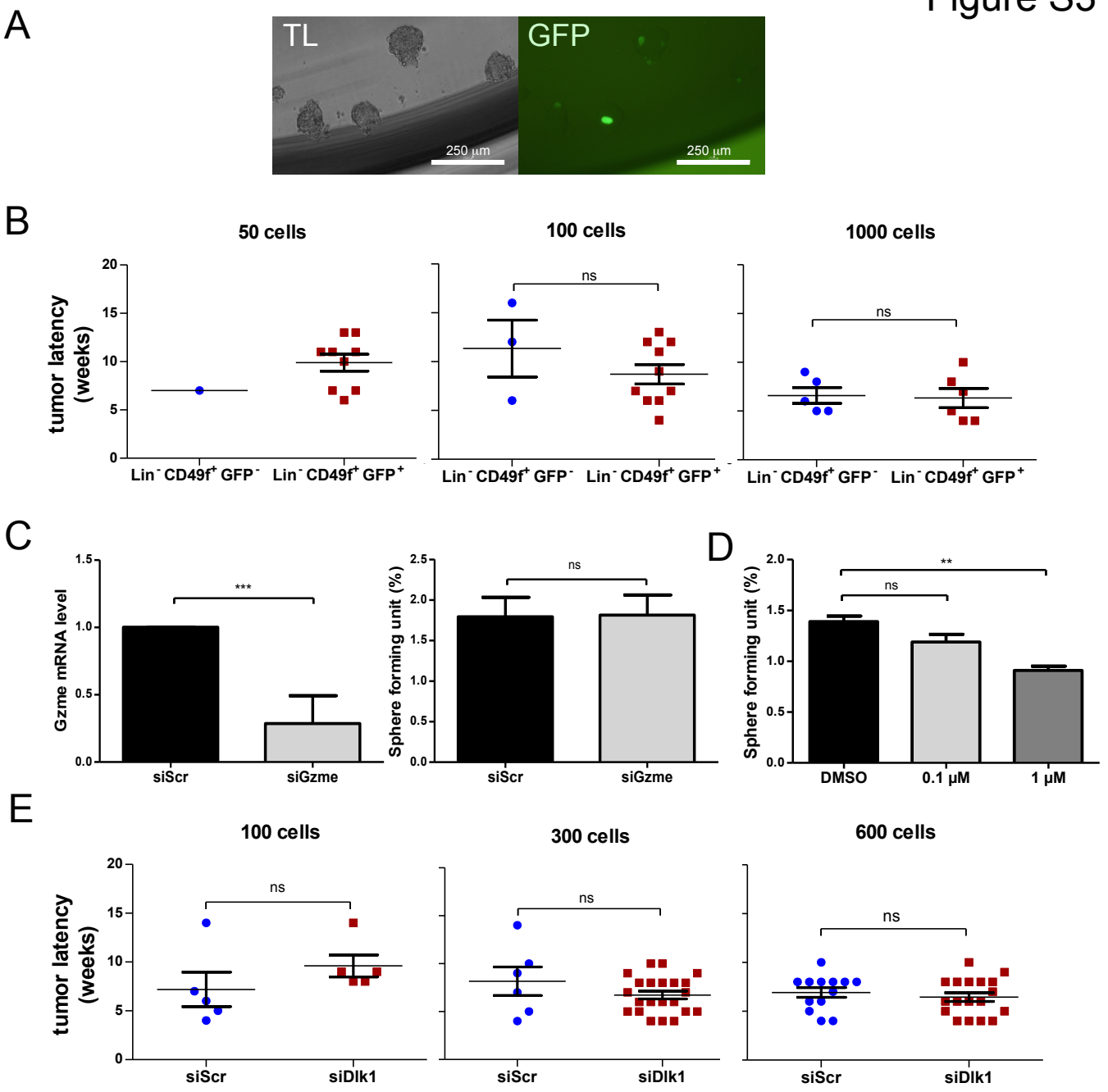

Figure S3. (A) Long-term maintenance of sphere-forming potential of s-SHIP/GFP$^+$ tumor cells (related to Figure 2), (B) tumor latency of primary injection of Lin$^-$CD49f$^+$GFP$^+$ cells in SCID mice (related to Figure 3A), (C) Inhibition of *Gzme* expression did not modify the sphere-forming potential of Lin$^-$CD49f$^+$GFP$^+$ tumor cells (related to Figure 4), (D) Notch signaling inhibition decreased sphere-forming potential of Lin$^-$CD49f$^+$GFP$^+$ cells (related to Figure 4), (E) Tumor latency of siScr- (control) and si*Dlk1*- treated Lin$^-$CD49f$^+$GFP$^-$ cells injected in SCID mice (related to Figure 4F).

(A) Spheres derived from GFP$^+$ cells can be maintained through at least four passages and GFP$^+$ cells persisted during sphere passaging (n=3 independent experiments). Representative photographs of spheres from the 4th passage was shown. Scale bar: 250 µm. **(B)** Tumor latency of primary injection in SCID mice; mice were monitored twice a week and tumor graft latency was measured as the time between implantation and the development of a palpable tumor. (**C**) si*Gzme* or control siScramble (siScr) were introduced into Lin$^-$CD49f$^+$GFP$^+$ cells isolated from bi-Tg mammary tumors. 48h after transfection, the level of *Gzme* mRNA was determined by RT-qPCR (left panel). siScr or si*Gzme* transfected Lin$^-$CD49f$^+$GFP$^+$ cells were plated under spheres conditions and spheres were numbered after 7 to 10 days in culture (right panel). Data represent mean values ± SEM of six independent experiments. (**D**) Lin$^-$CD49f$^+$GFP$^+$ cells were plated under spheres conditions in the presence of Compound E (0.1 µM or 1 µM) or carrier (DMSO). Data represent mean values ± SEM of four independent experiments. **(E)** Tumor latency of si*Dlk1*- or siScr-Lin$^-$CD49f$^+$GFP$^-$ cells injected in SCID mice; mice were monitored twice a week and tumor graft latency was measured as the time between implantation and the development of a palpable tumor. (**B-E**) *p* values were determined by Student's test ***$p<0.001$ **$p<0.01$ ns= not significant.

Supplemental Experimental Procedures

Mouse genotyping

FVB-Tg(C3-1-Tag)cJeg/JegJ mice were from Charles River Laboratories (L'Arbresle, France). FVB/N transgenic 11.5kb-GFP mice have been described previously (Rohrschneider et al, 2005, Brocqueville et al, 2010). FVB/N wild-type mice were from Janvier Labs (France) and CB17 SCID mice were from Institut Pasteur de Lille (France). Animals were housed and bred in accordance with institution guidelines for humane animal treatment. For genotyping of bi-transgenic mice, tail clips were digested in lysis buffer (KAPA Biosystems). Samples were diluted 1:10 and employed for PCR reactions to amplify T antigen cDNA using the primers TA1: 5'-GACCTGTGGCTGAGTTTGCTCA-3' and TA2: 5'-GCTTTATTTGTAACCATTATAAG-3'. Products of the amplification were analyzed by agarose gel electrophoresis.

Histology

Mammary tumors were fixed in 4% formaldehyde (ThermoFisher) at 4°C overnight, dehydrated in ethanol, and cleared in toluene. Dehydrated tumors were embedded in paraffin and cut into 4 µm sections. Tissue sections were dewaxed, rehydrated and stained with Hematoxylin and Eosin (Sigma). After staining, tissue sections were dehydrated and mounted with Eukitt® Quick-hardening mounting medium (Sigma). Images were acquired using bright field microscopy (Nikon).

Isolation of mammary tumor cells

Tumors were harvested from 4 to 6-month-old female bi-transgenic mice and minced using razor blades and digested using Mouse Tumor Dissociation Kit (Miltenyi Biotec) according to the manufacturer's instructions. After digestion, cells were filtered through 40µm cell strainers and washed once with washing buffer (DMEM medium) (Gibco). Then, cells were suspended in Red Blood Cell Lysis Solution (Miltenyi Biotec) in order to eliminate red blood cells. Cells were washed with PBS buffer (no Tris buffer and protein free), and were suspended in diluted Zombie Violet® solution (1/100, Zombie Violet™ Fixable Viability Kit, BioLegend) and incubated at room temperature, in the dark, for 15 minutes. Cells were washed once with complete medium (DMEM medium supplemented with 10% of bovine fetal serum (FBS) and 1X ZellShield ® (Minerva Biolabs). Then, cells were resuspended in complete medium before labeling with antibodies.

Flow cytometry, antibodies, and cell sorting

Single cells were preincubated with rat anti-mouse CD16/CD32 antibody (1:50; eBioscience #14-0161-85) for 10 min at 4°C, stained with antibodies for 30 min at 4°C with agitation, washed and resuspended in complete medium before analysis. Antibodies used were as follows: APC rat anti-human/mouse CD49f (1:100; eBioscience #17-0495-82), PE-Cy7 rat anti-mouse CD24 (1:100; Biolegend #101822), APC Armenian hamster anti-mouse CD29 (1:100; eBioscience #17-0291-82), Alexa Fluor 647 rat anti-mouse CD326 (EpCAM) (1:100; BioLegend #118212); and lineage markers PE rat anti-mouse CD31 (1:100; eBioscience #12-0311-83), PE rat anti-mouse CD45 (1:100; eBioscience # 12-0451-83), PE rat anti-mouse TER-119 (1:100; eBioscience #12-5921-83). The stained specimens were then analyzed or sorted using FACSAria flow cytometer (BD Biosciences). For data analysis, the horizontal and vertical lines of the gates were set using isotype and unstained controls. To define the GFP gate, tumor cells that do not express GFP were obtained from mammary tumors of 5-month-old FVB C3(1)Tag mice. Selection criteria that included side scatter and forward scatter profiles, depletion of zombie violet-positive cells and depletion of Lin-positive cells were used. Cells with appropriate GFP and CD49f status were then collected. After sorting, cells were washed with PBS and counted with trypan blue to exclude dead cells and determine cell numbers.

Tumor injection

SCID and FVB/N female mice (6–8 weeks of age) were sedated via inhalation of isoflurane (Baxter SAS, France). Sorted cells, transfected or not with siRNA, were suspended in 50µl of PBS, which was then mixed with 50µl of Growth Factor Reduced Matrigel (354230; BD Biosciences). The cell mixture was then injected subcutaneously in the region next to the nipple of the third thoracic gland of the mice using a 29G x 12.7 mm needle. Mice were observed weekly for 1–7 months for tumor formation. All tumorigenic cell frequencies were calculated using ELDA: Extreme Limiting Dilution Analysis (Hu and Smyth, 2009).

Mammosphere-forming assay

Single cell suspensions were plated at 25,000 cells/ml in serum-free DMEM/F12 medium, supplemented with 2% B27 (Invitrogen), 20 ng/ml FGF (Peprotech), 20 ng/ml EGF (Peprotech), 4 µg/ml heparin (Sigma), 5 µg/ml

insulin (Sigma) and 0.5μg/ml hydrocortisone (Sigma) for 7-14 days on 96-well ultra-low attachment plate (Corning). Cells were fed with fresh medium every three days and passaged using Trypsin/EDTA (Lonza). E-compound (Stem Cell Technologies) was dissolved in DMSO. Numbers and sizes of the mammospheres were determined under phase contrast microscopy. Only spheres that were larger than 50 μm were numbered. Sphere-forming potential was evaluated as follow: sphere-forming unit (SFU) = spheres/input cells x 100. Fluorescence microscopy was used to detect GFP-positive cells. Pictures were taken on a Zeiss Axio-Observer Z1 microscope.

RNA isolation and quantitative RT–PCR

Total RNA was extracted using the RNeasy Micro Kit (Qiagen). Reverse transcription (RT) was performed using QuantiTect Reverse Transcription kit (Qiagen) according to the manufacturer's instructions. Diluted cDNAs were transferred to 96-well PCR optical plates (Axygen). KAPA SYBR FAST qPCR kit (Kapa Biosystems) was used. qRT-PCR was performed using the Agilent Mx3000P detection system (Agilent Technologies). Relative mRNA levels were determined following normalization to the housekeeping genes: Actin, HPRT, Rpl38, and analysis of the comparative threshold cycle (2-ΔΔCt) method. Primer sequences were as follows: s-SHIP forward, 5'-GTTCCCACTAGTTGTTGAACTTTACCTT-3'; s-SHIP reverse, 5'-CAACGTCCACTTTGAGATGCAT-3'; GFP forward, 5'- AAGGCTACGTCCAGGAGCGCA -3'; GFP reverse, 5'- TGCCGTCCTCGATGTTGTGGC -3'; Actin forward, 5'- GATCTGGCACCACACCTTCT -3'; Actin reverse, 5'- GGGGTGTTGAAGGTCTCAAA -3'; HPRT forward, 5'- GAGAGCGTTGGGCTTACCTC -3'; HPRT reverse, 5'- ATCGCTAATCACGACGCTGG -3'; RPL38 forward, 5'- GGTTCTCATCGCTGTGCGG – 3'; RPL38 reverse, 5'- TGACAGACTTGGCATCCTTCC – 3'. Dlk1 forward 5'-GAAATAGACGTTCGGGCTTG-3'; Dlk1 reverse 5'-AGGGAGAACCATTGATCACG-3' ; Gzme forward 5'-CCACAACATCAAGGCTAAGG-3' Gzme reverse 5'- GCATGATGTCACTGAAGAAG –3'

Immunofluorescence and antibodies

Tumors were fixed in 4% paraformaldehyde overnight and put into 30% sucrose overnight, embedded in O.C.T., frozen on dry ice, and cut into 5-μm sections. Tissue sections were permeabilized with 0.5% Triton X-100, blocked with 5% FBS, and then incubated sequentially with primary antibodies overnight at 4°C, and with secondary antibodies for 45 min at room temperature. Slides were washed three times with PBS after each antibody incubation, and sections were mounted in Prolong Gold (Invitrogen). Primary antibodies used for this study were rabbit anti-cytokeratin 14 (1:500; Covance #PRB-155P), rat anti-cytokeratin 8 (1:100; Merk #MABT329, clone TROMA-1), Fluorochrome-conjugated secondary antibodies were Alexa Fluor 594 F(ab')2 fragment of goat anti-rabbit IgG (1:1000; Molecular Probes #A-11072) and Alexa Fluor 594 F(ab')2 fragment of goat anti-rat IgG (1:1000; Molecular Probes #A-11007). Sections were counterstained with DAPI (1 μg/mL; Sigma) to visualize cell nuclei. Pictures were taken on a LSM 710 confocal microscope (objectives Plan apochromat, Carl Zeiss, Germany).

Microarray analysis

Total RNA was prepared using the RNeasy micro kit (Qiagen) according to manufacturer's instructions, including the additional step of DNase treatment. Total RNA yield and quality were further assessed on a NanoDrop ND-1000 and an Agilent 2100 bioanalyzer (Agilent Technologies, Massy, France). One color whole Mouse (074809 slides) 60-mer oligonucleotides 8x60k microarrays (Agilent Technologies) were used to analyze gene expression. cRNA labeling, hybridization, and detection were carried out according to supplier's instructions (Agilent Technologies). For each microarray, Cyanine 3-labeled cRNA was synthesized with the low input QuickAmp labeling kit from 20ng of total RNA. RNA Spike-In was added to all tubes and used as positive controls of labeling and amplification steps. The labeled cRNA was purified and 600 ng of each cRNA were then hybridized and washed following manufacturer's instructions. Microarrays were scanned and data extracted using Agilent Feature Extraction Software© (FE version 10.7.3.1). Statistical comparisons and filtering were achieved with the Genespring® software version GX14.5 (Agilent Technologies). After a 75 percentile normalization of raw data, non-expressed probes in all conditions were removed, followed by a paired t-test with a p-value cut-off at 0.01 and a fold change cut off at +/-2. Further investigations were carried out using Ingenuity Pathway Analysis© Software (Ingenuity® Systems, www.ingenuity.com, Redwood City, CA, USA).

siRNA transfection

For *Dlk1* or *Gzme* knockdown analysis, dissociated and FACS-sorted $Lin^-CD49f^+GFP^-$ or $Lin^-CD49f^+GFP^+$ cells from the bi-transgenic tumors (10^5 cells/ well) were suspended into 24-well ultra-low attachment plates (Corning), and were transfected with ON-TARGET plus Non-targeting Pool as empty control and ON-TARGET plus *Dlk1* siRNA or ON-TARGET plus *Gzme* siRNA (Dharmacon-SMART pool) respectively, by using Lipofectamine RNAiMAX (Life Technology) for 45 min in a final volume of 500 μL serum-free mammosphere medium. The transfected cells were then collected and washed once with mammosphere medium in order to

remove transfection reagent and siRNA. Cells were counted and suspended in mammosphere medium (500 or 2000 cells/well) into 96-well ultra-low attachment plates. The sphere-forming potential was analyzed 7-10 days after culture. Downregulation of *Dlk1* or *Gzme* mRNA was verified by RT-qPCR 2 days and 8 days after transfection.